ChemComm

ROYAL SOCIETY OF CHEMISTRY

COMMUNICATION

View Article Online
View Journal | View Issue

Check for updates

Cite this: *Chem. Commun.*, 2024, **60**, 13710

Received 31st August 2024,
Accepted 29th October 2024

DOI: 10.1039/d4cc04477k

rsc.li/chemcomm

Published on 31 October 2024. Downloaded on 1/14/2026 12:48:58 PM.

Superhydrophobic PVDF/SiO_2 composite films with a hierarchical structure for highly stabilized radiative cooling†

Zhengfei Tan,[ac] Huiyu Yang,*[a] Xiaohua Cheng,[a] Guowen Yu,[a] Hai Liu,[a] Bingqing Zhang *[b] and Chunli Gong[a]

PVDF/SiO_2 composite films with a hierarchical structure were prepared by water bath solvent exchange and they realized the integration of self-cleaning and radiative cooling. The high scattering properties of SiO_2 effectively enhanced the radiative cooling performance of the films, and the weathering stability of the composite films was evaluated by UV radiation treatment and friction resistance analysis.

Passive daytime radiant cooling has received significant attention as a sustainable method to reduce the temperature of materials with zero energy consumption.[1,2] Radiatively cooled materials under direct sunlight not only reflect the sunlight with wavelengths of 0.3–2.5 μm, but also emit heat within an atmospheric window of 8–13 μm into cold outer space. Therefore, the requirements of high solar reflectance and strong mid-infrared emissivity must be met to achieve radiative cooling. The former reduces the solar heat gain, while the latter increases the radiative heat gain in outer space.[3–5] To date, many studies have reported high reflectivity and high emissivity coatings with good effects, including photonic materials,[6–8] inorganic powder materials,[9,10] metal–polymer layered coatings,[11,12] porous polymer coatings[13,14] or aerogels[15] and textiles with nanostructures[16,17] or nanoparticles.[18] These studies have gradually expanded the application areas of radiative cooling technology.

However, passive radiative cooling still faces many challenges in practical applications, such as how to prepare photonic crystals simply and efficiently,[19] colorization of highly radiatively cooled materials,[20] preparation of radiative cooling materials with self-cleaning surfaces[21] and high UV resistance,[22] *etc.* In particular, the accumulation of dust or other particulate contaminants affects the cleanliness of the materials' surface, reducing the surface reflectance and emissivity, thereby affecting the cooling performance of the materials.

Herein, we prepared superhydrophobic radiation-cooled composite films consisting of PVDF (polyvinylidene fluoride) and gas-phase hydrophobic SiO_2 nanoparticles by solvent exchange. The synergistic effect of the porous layered structure and the high light-scattering properties of SiO_2 enabled the composite films to achieve strong reflection of sunlight to reduce radiant heat, maximum emission of radiant heat through the atmospheric window, and self-cleaning to prevent surface contamination. More importantly, the radiative cooling composite films retain high radiative cooling performance under strong UV radiation, thus showing effectively improved durability and stability for outdoor applications.[23]

The preparation of PVDF/hydrophobic nano-SiO_2 composite films with a hierarchical porous structure by water bath solvent exchange is illustrated in Fig. S1 (ESI†). During this process, the high reflection of SiO_2 microspheres not only improves the radiative cooling effect of the composite films but also effectively regulates the size and distribution of the porous structure and reduces the thermal aggregation of the composite films. Compared with the pure PVDF film (Fig. S2, ESI†), the SiO_2-added composite film exhibits a superior porous hierarchical structure and static water contact angle as depicted in Fig. 1. The pore size of the PVDF–10% SiO_2 composite membrane was significantly higher than that of the PVDF–5% SiO_2 composite membrane, and a large number of nanoparticles were loaded in the pores and pore walls (Fig. 1b). Meanwhile, the micro/nano-hierarchical structure of the surface of the PVDF–10% SiO_2 composite film resulted in a higher contact angle of 150° (inset of Fig. 1b). The cross-section shows that the thickness of the composite film is about 273 μm (Fig. S3, ESI†). As the SiO_2 content increased from 10% to 20%, the porous structure of the

[a] *School of Chemistry and Materials Science, Hubei Engineering University, Xiaogan 432000, China. E-mail: hy-yang_wtu@hotmail.com*
[b] *State Key Laboratory of Marine Resource Utilization in South China Sea, School of Materials Science and Engineering, Hainan University, HaiKou 570228, China. E-mail: bqzhang@hainanu.edu.cn*
[c] *Ministry of Education Key Laboratory for the Green Preparation and Application of Functional Materials, Hubei Key Laboratory of Polymer Materials, School of Materials Science and Engineering, Hubei University, Wuhan 430062, China*

† Electronic supplementary information (ESI) available: Experimental section and supporting figures and tables. See DOI: https://doi.org/10.1039/d4cc04477k

This journal is © The Royal Society of Chemistry 2024

Published on 31 October 2024. Downloaded on 1/14/2026 12:48:58 PM.

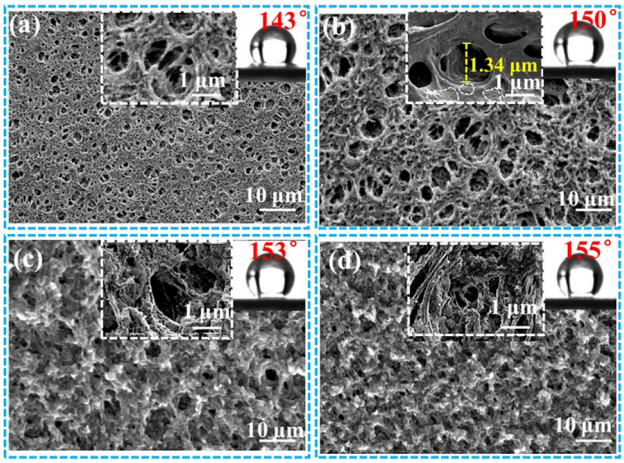

Fig. 1 Surface micromorphology and static water contact angle of PVDF–n% SiO_2 composite films: (a) PVDF–5% SiO_2; (b) PVDF–10% SiO_2; (c) PVDF–15% SiO_2; (d) PVDF–20% SiO_2.

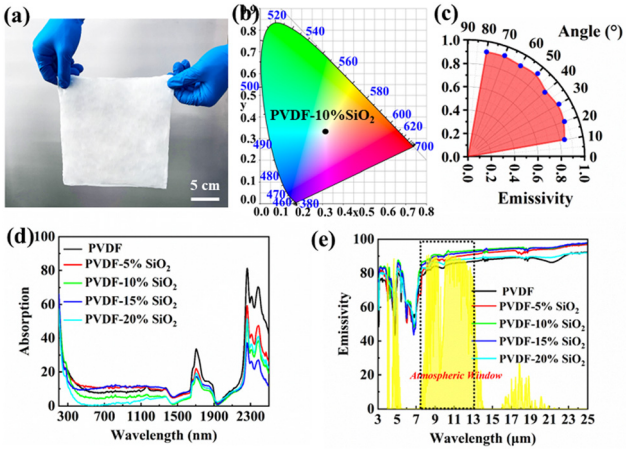

Fig. 2 (a) and (b) Optical photographs and CIE chromaticity coordinates of the PVDF–10% SiO_2 composite film, respectively; (c) average emissivity of the PVDF–10% SiO_2 composite film in the atmospheric window at different polarization angles; (d) absorption spectra of PVDF and PVDF–n% SiO_2 in the UV-vis-NIR region; (e) IR emission spectra of PVDF and PVDF–n% SiO_2.

composite film gradually decreased and the micro/nano-surface roughness of the structure gradually increased. The inner pores and pore walls of the PVDF–20% SiO_2 composite film were almost completely covered by nanoparticles when the SiO_2 content was 20% (Fig. 1d). The surface static water contact angle reached a maximum of 155° (inset of Fig. 1d). This indicates that the incorporation of hydrophobic SiO_2 nanoparticles can not only modulate the hierarchical structure of PVDF films, but also significantly enhance the super-hydrophobicity of the film surface.

The surface roughness and surface energy of PVDF and PVDF–n% SiO_2 films are shown in Fig. S4 and S5 (ESI†). The hydrophobic SiO_2 nanoparticles not only improved the roughness of the PVDF film, but also effectively reduced the surface energy, thus improving the surface hydrophobicity of the PVDF–n% SiO_2 composite films. The dye easily slipped off the surface of the PVDF–10% SiO_2 composite film without staining, as displayed in Fig. S4g (ESI†). Meanwhile, liquid droplets such as deionized water, milk, potassium permanganate solution, phenolphthalein and tea water showed an approximately spherical shape on the surface of the PVDF–10% SiO_2 composite film, indicating its excellent super-hydrophobicity (Fig. S4h, ESI†).

The bright white color indicates a strong scattering or reflecting effect on visible light. The CIE colorimetric coordinate analysis was further confirmed as indicated in Fig. 2b. The L^*, a^*, and b^* values of the PVDF/SiO_2 composite film were 94.87, −0.01, and 3.16, respectively. The strong scattering effect can reduce the thermal gain of the composite film, thus improving the cooling performance. In addition, the average emissivity of the PVDF–10% SiO_2 composite film is greater than 0.9 over a wide range of polarization angles from 10° to 80° in the atmospheric window (Fig. 2c), indicating that the composite film emits heat flux to outer space efficiently and stably. This can be attributed to the porous hierarchical structure of the PVDF–10% SiO_2 composite film surface in different directions. The porous structure of the film does not match the refractive index of the air inside the holes, which results in a strong scattering of sunlight.[24] In the range of 200–2500 nm, the average absorption percentages of PVDF, PVDF–5% SiO_2, PVDF–10% SiO_2, PVDF–15% SiO_2 and PVDF–20% SiO_2 are 17.18%, 14.37%, 10.4%, 12.3% and 9.15%, respectively (Fig. 2d). This may be attributed to the light scattering effect of SiO_2 and the diffuse reflecting effect of the pores, reducing the average absorptivity of the PVDF films. Meanwhile, both PVDF and PVDF–n% SiO_2 films displayed strong thermal emission in the wavelength range of 2.5–25 μm (Fig. 2e). The average emissivity of the PVDF film in the atmospheric window (0.84) was significantly lower than those of PVDF–n% SiO_2 films. Compared to the average emissivity of the PVDF–20% SiO_2 composite film (0.86), the average emissivity of the PVDF–10% SiO_2 film in the atmospheric window was higher (0.93). The high emissivity of the PVDF–n% SiO_2 films was caused by the C–F vibrations in the PVDF molecules and multiple reflections in the pore structure increased the absorption.[24] In addition, the phonon–polariton resonance of Si–O bonds at 9.7 μm and SiO_2 agglomerates also enhance the absorption in the mid-infrared region.[25,26] Therefore, considering the hierarchical structure and optical properties, we selected the composite film with 10% SiO_2 content for the radiative cooling performance study.

The radiative cooling performance of the films was practically evaluated by using a homemade device (Fig. 3). The temperatures of the cavities covered with the PVDF film, PVDF/SiO_2 composite film (PVDF–10% SiO_2), commercially cooled film and PE film were measured under direct sunlight. The surface of the device was covered with PE film and aluminum foil to reduce the heat transfer between the sample and the environment (Fig. 3a). As shown in Fig. 3c, the average temperatures of the cavities covered by the PVDF film, PVDF/SiO_2 composite film, commercial film and PE film were 35.1 °C, 31.7 °C, 37.7 °C and 43.2 °C, respectively, at the solar irradiation intensity of 1000 W m^{-2}. Compared to the temperatures of the cavities covered by the commercial film and PE films, the

Published on 31 October 2024. Downloaded on 1/14/2026 12:48:58 PM.

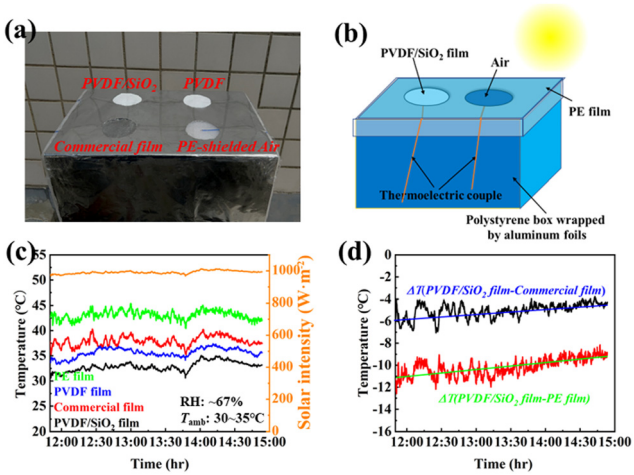

Fig. 3 (a) Photograph of the homemade radiative cooling performance test device; (b) schematic diagram of the radiative cooling temperature test device; (c) outdoor real-time recordings of sunlight intensity and temperatures of cavities covered by PVDF films, PVDF/SiO_2 composite films, commercial cooling films and PE films (July 12, 2023, Xiaogan, China, 30° 55′N, 113° 54′E, RH: ~67%, T_{amb}: 30–35 °C); (d) temperature difference between the PVDF/SiO_2 composite film and the cavities covered by commercial and PE films, respectively.

temperature of the cavities covered by the PVDF/SiO_2 composite films decreased by about 6.0 °C and 11.5 °C, respectively (Fig. 3d). Fig. S6 (ESI†) reveals that the cooling power of the PVDF/SiO_2 composite film was 114.3 W m^{-2}, while the cooling power of the PVDF film was only 102.7 W m^{-2}. Meanwhile, the cooling capabilities of PVDF and PVDF/SiO_2 composite films were compared for practical outdoor applications (Fig. S7, ESI†). The average surface temperature of the exposed part of the bicycle seat under direct sunlight reached 58.1 °C, while the average temperatures of the part covered by PVDF film and PVDF/SiO_2 composite film were 39.8 °C and 35.1 °C, respectively (Fig. S7e, ESI†). The surface temperature of the bicycle seat covered by the PVDF/SiO_2 composite film was further reduced by 4.7 °C compared to that of the bicycle seat covered by the PVDF film (Fig. S7f, ESI†). In addition, the surface temperature of the film was observed to be only 28.8 °C after the PVDF/SiO_2 composite film was placed on the hand under direct sunlight for 5 min (Fig. S7d, ESI†). The above results indicate that the synergistic effect of PVDF with a hierarchical structure and SiO_2 nanoparticles can further enhance the radiative cooling performance of the films.[27,28]

Thermal conductivity is an important factor affecting the heat gain of the film. Low thermal conductivity reduces the diffusion of optical radiant heat, realizes low thermal aggregation in the film, and effectively reduces the surface temperature of the covered substrate.[4,29–31] Fig. S8b (ESI†) shows that the PVDF film with added SiO_2 nanoparticles has a lower thermal conductivity compared to the PVDF film. The PVDF/SiO_2 composite film with 10% SiO_2 has the lowest thermal conductivity of 0.09 W m^{-1} K^{-1}. This is mainly attributed to the excellent porous hierarchical structure of the PVDF–10% SiO_2 composite film. Subsequently, the radiative cooling was compared with a high reflectance silk fabric under a xenon lamp (Fig. S8, ESI†). The results showed that the average temperature drop ΔT of the PVDF/SiO_2 film was 6.5 °C, while the average temperature drop ΔT of the silk fabric was only 2.6 °C (Fig. S8c, ESI†). This temperature difference confirms that the PVDF/SiO_2 film has a higher light reflectivity. Meanwhile, the equilibrium temperature of the surface of silk fabric is higher than its corresponding covered cavity temperature by 4.9 °C (Fig. S8c, ESI†), while it is higher than 2.5 °C and 1 °C for the PVDF film and PVDF/SiO_2 film, respectively. This suggests that the PVDF/SiO_2 film with a hierarchical structure has a lower heat gain and shows rapid heat diffusion into the environment (Fig. S8d, ESI†).

The PVDF/SiO_2 composite films were rubbed reciprocally on a 400-mesh sandpaper surface to evaluate the mechanical stability,[32] as shown in Fig. S9a (ESI†). After 50 rubbing cycles, the PVDF/SiO_2 composite film remained highly hydrophobic with a contact angle of 150° (Fig. S9b, ESI†). The outdoor radiative cooling performance of the PVDF/SiO_2 composite films was then compared with that of commercial films after 50 rubbings. The results show that the average temperature drop ΔT of the PVDF/SiO_2 composite film compared to that of the commercial film is 4.8 °C at an average solar intensity close to 970 W m^{-2} (Fig. S9e, ESI†). The average temperature difference between the PVDF/SiO_2 composite film before abrasion and the commercial film under 1000 W m^{-2} direct sunlight is only slightly higher than that after abrasion (a ΔT of 6.0 °C, Fig. 3c) without considering the angle of solar radiation and ambient heat exchange. These results indicate that the PVDF/SiO_2 composite films have excellent mechanical stability. In addition, the excellent flexibility of the PVDF/SiO_2 composite films can accommodate different degrees of folding deformation, thus meeting the cooling requirements of different shapes of materials' surfaces (Fig. S9c, ESI†).

The stability and durability effects of the radiative cooling performance of the composite films were evaluated by UV aging. The surface of the PVDF/SiO_2 composite film still retains excellent hydrophobicity after 20 h of continuous radiation under strong UV light (400 W m^{-2}) as depicted in Fig. 4a. Meanwhile, the tensile stress of the PVDF/SiO_2 composite film decreases by only 3.2% (Fig. 4b), which further indicates that the composite film has strong UV resistance. Fig. 4c displays the radiative cooling performance of PVDF/SiO_2 composite films after UV radiation evaluated under xenon lamp simulated sunlight. The results reveal that the cooling performance of the PVDF/SiO_2 composite films before and after UV radiation is almost unchanged. The average temperature drop ΔT of the PVDF/SiO_2 composite film after UV radiation reaches 7.9 °C compared to the average temperature of PE-covered air (Fig. 4d). In addition, the outdoor radiative cooling performance of PVDF/SiO_2 composite films was evaluated under strong UV light irradiation (400 W m^{-2}) for 168 h (Fig. S10a, ESI†). The cooling temperature of PVDF/SiO_2 composite films before and after UV radiation still did not change significantly, indicating a high cooling effect. Meanwhile, the stress of the PVDF/SiO_2 composite films after 168 h of UV radiation decreased only by 2.3% and the strain increased by 1.2%

 This journal is © The Royal Society of Chemistry 2024

Published on 31 October 2024. Downloaded on 1/14/2026 12:48:58 PM.

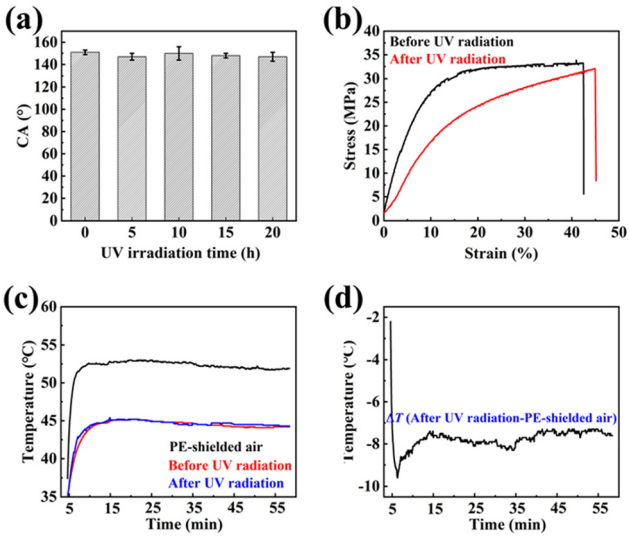

Fig. 4 (a) Contact angle of PVDF/SiO_2 composite films at different UV aging times; (b) stress–strain curves of PVDF/SiO_2 composite films before and after UV radiation (radiation for 20 h); (c) real-time temperature profiles of PVDF/SiO_2 composite films under a xenon lamp before and after UV radiation; (d) average temperature drop (ΔT) of the PVDF/SiO_2 composite film after UV radiation and PE covered air.

compared with that of 20 h of radiation (Fig. S10b, ESI†). The above results confirm that the PVDF/SiO_2 composite films show radiative cooling performance with excellent stability under strong UV radiation and can better meet the needs of practical applications.

In summary, PVDF and hydrophobic SiO_2 nanoparticles were used to prepare superhydrophobic radiation-cooled thin films with a hierarchical porous structure by a solvent exchange method. The average infrared emissivity of the PVDF/SiO_2 composite films in the atmospheric window was 0.93 and was greater than 0.9 in the polarization angle range from 10° to 80°. Compared to the temperatures of the cavities covered by the commercial film and PE films, the temperature of the cavities covered by the PVDF/SiO_2 composite films decreased by about 6.0 °C and 11.5 °C under 1000 W m^{-2} solar irradiation intensity conditions, respectively. Meanwhile, the PVDF/SiO_2 composite film shows excellent self-cleaning performance and UV resistance, which is favourable for the film's sustainable outdoor radiation cooling practical applications. This approach provides a practical, efficient and sustainable new way for the design of energy-free radiative cooling materials.

This work was supported by the Hubei Key Laboratory of Biomass Fibers & Eco-Dyeing & Finishing (Wuhan Textile University) (SWJ202207) and the Natural Science Foundation of Xiaogan (Grant XGKJ2023010059).

Data availability

All data supporting this research are included in the main article and/or ESI.†

Conflicts of interest

There are no conflicts to declare.

Notes and references

1 X. Yin, R. Yang, G. Tan and S. Fan, *Science*, 2020, **370**, 786–791.
2 J.-H. Wang, C.-H. Xue, B.-Y. Liu, X.-J. Guo, L.-C. Hu, H.-D. Wang and F.-Q. Deng, *ACS Omega*, 2022, **7**, 15247–15257.
3 Y. Ma, *Nature*, 2020, **577**, 18–20.
4 D. Zhao, A. Aili, Y. Zhai, S. Xu, G. Tan, X. Yin and R. Yang, *Appl. Phys. Rev.*, 2019, **6**, 021306.
5 B. Zhao, M. Hu, X. Ao, N. Chen and G. Pei, *Appl. Energy*, 2019, **236**, 489–513.
6 E. Rephaeli, A. Raman and S. Fan, *Nano Lett.*, 2013, **13**, 1457–1461.
7 A. P. Raman, M. A. Anoma, L. Zhu, E. Rephaeli and S. Fan, *Nature*, 2014, **515**, 540–544.
8 Z. Chen, L. Zhu, A. Raman and S. Fan, *Nat. Commun.*, 2016, **7**, 13729.
9 G. Chen, Y. Wang, J. Qiu, J. Cao, Y. Zou, S. Wang, D. Jia and Y. Zhou, *ACS Appl. Mater. Interfaces*, 2020, **12**, 54963–54971.
10 D. Chae, M. Kim, P.-H. Jung, S. Son, J. Seo, Y. Liu, B. J. Lee and H. Lee, *ACS Appl. Mater. Interfaces*, 2020, **12**, 8073–8081.
11 B. Bhatia, A. Leroy, Y. Shen, L. Zhao, M. Gianello, D. Li, T. Gu, J. Hu, M. Soljačić and E. N. Wang, *Nat. Commun.*, 2018, **9**, 5001.
12 L. Zhou, H. Song, J. Liang, M. Singer, M. Zhou, E. Stegenburgs, N. Zhang, C. Xu, T. Ng and Z. Yu, *Nat. Sustainability*, 2019, **2**, 718–724.
13 H. Zhao, Q. Sun, J. Zhou, X. Deng and J. Cui, *Adv. Mater.*, 2020, **32**, 2000870.
14 Y. Chen, J. Mandal, W. Li, A. Smith-Washington, C.-C. Tsai, W. Huang, S. Shrestha, N. Yu, R. P. Han and A. Cao, *Sci. Adv.*, 2020, **6**, eaaz5413.
15 A. Leroy, B. Bhatia, C. C. Kelsall, A. Castillejo-Cuberos, M. Di Capua H, L. Zhao, L. Zhang, A. Guzman and E. Wang, *Sci. Adv.*, 2019, **5**, eaat9480.
16 P.-C. Hsu, A. Y. Song, P. B. Catrysse, C. Liu, Y. Peng, J. Xie, S. Fan and Y. Cui, *Science*, 2016, **353**, 1019–1023.
17 X. Wang, X. Liu, Z. Li, H. Zhang, Z. Yang, H. Zhou and T. Fan, *Adv. Funct. Mater.*, 2020, **30**, 1907562.
18 S. Zeng, S. Pian, M. Su, Z. Wang, M. Wu, X. Liu, M. Chen, Y. Xiang, J. Wu and M. Zhang, *Science*, 2021, **373**, 692–696.
19 D. Chae, S. Son, Y. Liu, H. Lim and H. Lee, *Adv. Sci.*, 2020, **7**, 2001577.
20 S. Yu, Q. Zhang, Y. Wang, Y. Lv and R. Ma, *Nano Lett.*, 2022, **22**, 4925–4932.
21 M.-C. Huang, C.-H. Xue, J. Huang, B.-Y. Liu, X.-J. Guo, Z.-X. Bai, R.-X. Wei, H.-D. Wang, M.-M. Du and S.-T. Jia, *Chem. Eng. J.*, 2022, **442**, 136239.
22 X. Li, L. Pattelli, Z. Ding, M. Chen, T. Zhao, Y. Li, H. Xu, L. Pan and J. Zhao, *Adv. Funct. Mater.*, 2024, 2315315.
23 Z. Qin, M. Li, J. Flohn and Y. Hu, *Chem. Commun.*, 2021, **57**, 12236–12253.
24 C.-H. Xue, R.-X. Wei, X.-J. Guo, B.-Y. Liu, M.-M. Du, M.-C. Huang, H.-G. Li and S.-T. Jia, *Compos. Sci. Technol.*, 2022, **220**, 109279.
25 Y. Zhai, Y. G. Ma, S. N. David, D. L. Zhao, R. N. Lou, G. Tan, R. G. Yang and X. B. Yin, *Science*, 2017, **355**, 1062–1066.
26 X. Wang, X. H. Liu, Z. Y. Li, H. W. Zhang, Z. W. Yang, H. Zhou and T. Fan, *Adv. Funct. Mater.*, 2020, **30**, 1907562.
27 F. Xu, F. Wang and J. Ou, *Colloids Surf., A*, 2023, **676**, 132121.
28 D. Kumar, L. Li and Z. Chen, *Prog. Org. Coat.*, 2016, **101**, 385–390.
29 Y. Gao, X. Song, A. S. Farooq and P. Zhang, *Sol. Energy*, 2021, **228**, 474–485.
30 P. Poredoš, H. Shan, C. Wang, Z. Chen, Z. Shao, F. Deng, H. Liu, J. Yu and R. Wang, *Energy Environ. Sci.*, 2024, **17**, 2336–2355.
31 D. Zhao, A. Aili, Y. Zhai, J. Lu, D. Kidd, G. Tan, X. Yin and R. Yang, *Joule*, 2019, **3**, 111–123.
32 H. Sun, F. Yang, S. Chen and J. Zhang, *Composites, Part A*, 2023, **175**, 107750.